Scientia Iranica B (2023) 30(2), 409–427

Sharif University of Technology
Scientia Iranica
Transactions B: Mechanical Engineering
http://scientiairanica.sharif.edu

Energy, exergy, and economic analyses of geothermal power generation cycle with different organic fluids

F. Mehran[a,*], Y. Parvizifard[b], F. Hassanzadeh[a], and N. Kuznetsov[c]

a. *Department of Mechanical Engineering, Islamic Azad university, Jolfa International Branch, Jolfa, Iran.*
b. *Department of Mechanics, University College of Nabi Akram, Tabriz, Iran.*
c. *Financial University under the Government of the Russian Federation, Moscow, Russia.*

Received 20 March 2022; received in revised form 28 June 2022; accepted 21 November 2022

KEYWORDS
Geothermal energy;
Combined cycle;
Rankine cycle;
Single-effect evaporation cycle;
Double-effect evaporation cycle.

Abstract. In the present research, energy derived from the geothermal fluid is utilized to generate power. In the first case of power generation, the model of the geothermal double-effect instantaneous evaporation cycle is employed, while in the second one, the single-effect evaporation combined cycle and Rankine cycle with different organic fluids are utilized. The effect of several organic fluids in the combined cycle is then examined. The SPECO method was then incorporated in the economic analysis. According to the mentioned analysis, net power generation reached its maximum value for the combined cycle with water vapor and its minimum value for the double-effect instantaneous evaporation cycle with a considerable difference. Throughout the experiments, increasing the separator pressure at the constant evaporator temperature reduced the power generation cost for combined cycles. The lowest power generation cost was attributed to the combined cycle with operating fluid R113 while the highest amount of power generation cost was related to the combined cycle with ammonia fluid. The exergoeconomic coefficient, i.e., the ratio of the purchase price components to the sum of costs associated with total exergy destruction as well as the cost associated with purchasing cycle components, was also the highest in the combined cycle with R113 and the lowest in the double-effect instantaneous evaporation cycle.

© 2023 Sharif University of Technology. All rights reserved.

1. Introduction

Lately, exhaustion of fossil fuels, diversification of energy sources, sustainable development and energy security, and the consequent environmental issues resulting from fossil energy consumption on the one hand, and clean and renewable energy sources such as solar, wind, geothermal on the other hand, have encouraged the world to pay serious attention to the advancement and expansion of the renewable energy and to raise the share of these resources in the global energy worldwide. Nowadays, the world is experiencing a substantial increase in the activities and budgets of governments and companies in the arena of research, development, and provision of renewable energy systems [1–3]. These activities and investments will reduce the price of renewable energies over time, and these energies will be able to compete with the existing traditional energy systems. For instance, this objective has been accomplished in the case of wind energy and some applications of biomass energy, and the remarkable decline in prices for other renewable energy sources is still in progress [4,5]. As demonstrated in Figure 1,

*. *Corresponding author.*
E-mail address: Farshidmehran57@yahoo.com (F. Mehran)

10.24200/sci.2022.60156.6632

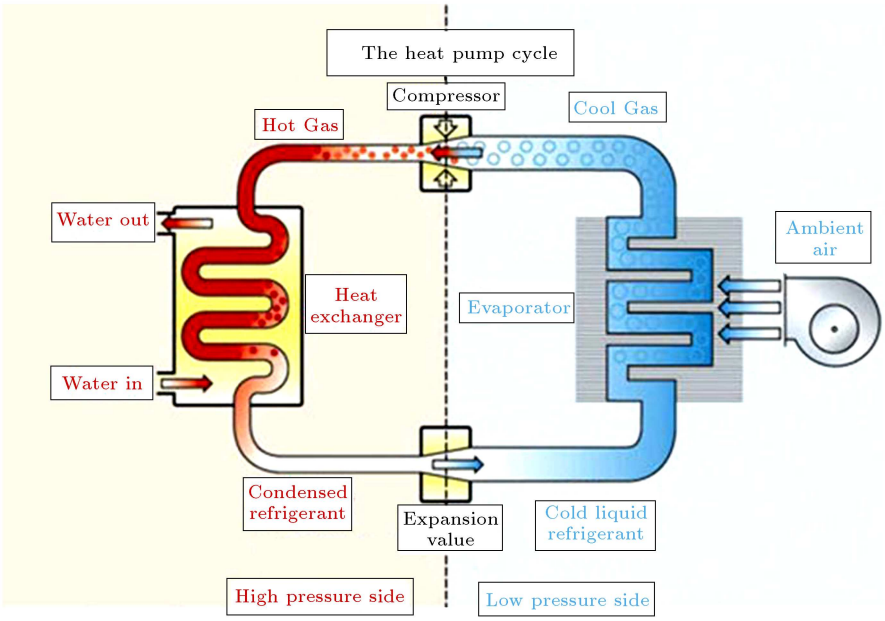

Figure 1. Heat pump with a geothermal fluid.

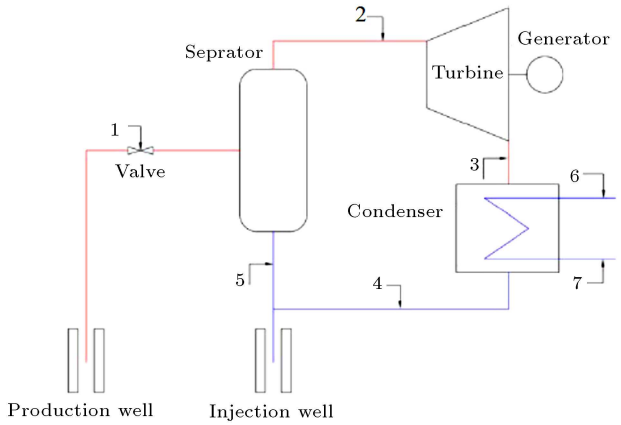

Figure 2. Geothermal single-effect evaporation cycle.

geothermal cooling and heating systems, known as a Geothermal Heat Pump (GHP), Geothermal Exchange systems (Geo Exchange), or Earth Energy Systems, consist of heat pumps that consume electricity to collect heat from the basement and transfer it to the unit installed inside the building by the fluid passing through the installed pipes.

Several research pieces have been conducted on the energy analysis and exergy of geothermal power generation cycles thus far, which will be examined in the next sections. Figure 2 depicts the geothermal single-effect evaporation cycle. Ehyaei et al. [6] analyzed the single-effect and double-effect power generation cycles in terms of exergy and obtained exergy efficiencies of 38.7 and 49% for the single-effect and double-effect cycles, respectively. In this analysis, a geothermal fluid of 250°C and condenser temperature of 40°C were utilized. An exergy analysis of a binary geothermal cycle with a capacity of 12.4 MW was carried out in [7], and the exergy efficiency and contribution of all cycle components to the exergy destruction of the whole cycle were acquired. Yari [8] examined the energy and exergy of different arrangements of the Organic Rankine Cycle (ORC) cycle to apply the energy of the high-temperature geothermal fluid and, finally, compared these cycles in terms of energy and exergy. Over the course of this survey, the highest efficiency of the first law for the ORC cycle with internal heat exchanger and operating fluid R123 was obtained as 7.65%. According to DiPippo's research [9], in case the geothermal binary cycle functions with a low-temperature geothermal fluid, it would still possess a high exergy efficiency rate of roughly 40%. Walraven et al. [10] thermodynamically compared the performance of various ORC and Kalina cycles to make use of a geothermal fluid source in the temperature range of 100–150°C. In their study, the best cycle exergy efficiency was calculated as more than 50%, which is considered high efficiency. Jalilinasrabady et al. [11] investigated the instantaneous single-effect and double-effect power generation cycles of Sabalan geothermal plant. According to their obtained results, if the separator and condenser pressure were considered equal to 5.5 and 0.3 bar, respectively, the net generation capacity of the single-effect evaporation cycle would reach 31 MW. In addition, if the first and second separator pressures and condenser pressures in the case of a double-effect evaporation cycle were equal to 7.5, 1/1, and 0.1, respectively, the net generation capacity of the cycle would reach 49.7 MW [12]. Figure 3 illustrates the geothermal instantaneous double-effect evaporation cycle.

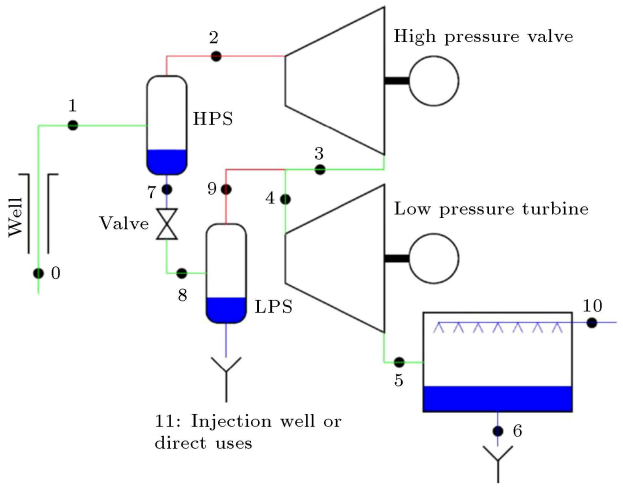

Figure 3. Geothermal instantaneous double-effect evaporation cycle.

Mohammadi et al. [13] optimized the Rankine cycle with an organic fluid with a geothermal heat source. In their study, they took into account the ratio of the cross-sectional area of the heat exchanger to the net power output as a target function and optimized the cycle. Liu et al. [14] analyzed the sensitivity of the functional parameters of the Rankine binary cycle with organic fluids. The cycle schematic is depicted in Figure 3 according to which the temperature of the geothermal fluid has the most significant impact on the cycle followed by the second most influential parameter in the thermodynamic performance of the binary cycle, i.e., evaporation temperature. In this research, thermodynamic optimization was performed, and the optimal values for the selected parameters were obtained. In another study, Wang et al. [15] investigated the transcritical cycle of carbon dioxide with geothermal fluid actuators using natural gas as a thermal sink. They found that at a certain inlet pressure to the turbine, the cycle exergy efficiency would reach the maximum value in different cases. Tempesti and Fiaschi [16] provided a combined cycle of simultaneous power and heat generation with renewable energy actuators. According to their observations, this cycle with R245fa operating fluid held the lowest power generation cost among the operating fluids examined in this combined cycle.

A review of the previous researches [17–20] on geothermal cycles reveals that comprehensive research on the geothermal power generation cycles is required in which two-effect rapid evaporative geothermal power generation cycles and a combined cycle of geothermal fluid with ORC cycle with different operating fluids are considered from the thermoeconomic point of view. In this regard, the present study analyzed and compared the two-effect instantaneous evaporative geothermal power generation cycles and combined single-effect evaporation geothermal cycle-Rankine cycle with different organic fluids in terms of energy and exergy [21,22]. Subsequently, a complete thermoeconomic analysis was done on the studied cycles and all thermoeconomic parameters, including the cost of power generation in turbines, costs related to the exergy destruction of all components, analysis of the exoeconomic parameters (f, r), and fuel and product costs. In the end, parametric analysis was carried out on the cycles, and the effect of different parameters on the energy, exergy, and economic performance of cycles was evaluated. In this study, organic fluids including n-heptane, R141b, R113, steam, and NH_3 were investigated as the ORC cycle operating fluids [23,24]. Further, the most efficient cycle and operating fluid were selected among the cycles and fluids considering the different energy, exergy, and economy factors. In addition, an answer was given to the question of whether or not a particular cycle and a fluid have the most favorable conditions from all three perspectives of energy, exergy, and economy, or different cycles and fluids. A review of the related sources indicates that the geothermal power generation cycle of the double-effect instantaneous evaporation and geothermal fluid combined cycle with ORC cycle with different operating fluids have not been comprehensively studied from a thermo-economic perspective.

2. Methodology

Contrary to energy, exergy is not stored but is destructed due to irreversibility. Physical exergy is proportional to the work that can be performed to transfer a system from its initial state to a state in mechanical and thermal equilibrium with the environment. In fact, the whole problem-solving method for energy, exergy, and economic analysis will be the same, as shown in Figure 4.

Meanwhile, chemical exergy is proportional to the work that can be done to transfer a system in mechanical and thermal equilibrium with the environment to a state with the most stable structure in equilibrium with the environment. The equilibrium of mass, energy, and exergy can be expressed as follows [25,26]:

$$\sum \dot{m}_i = \sum \dot{m}_e, \tag{1}$$

$$\dot{Q} + \sum \dot{m}_i h_i = \dot{W} + \sum \dot{m}_e h_e, \tag{2}$$

$$\dot{E}_Q + \sum \dot{m}_i h_i = \dot{E}_w + \sum \dot{m}_e h_e + \dot{E}_D, \tag{3}$$

where $\dot{m}$ is the mass flow rate (mass value of the fluid passing through a section per second, kg/s), $\dot{Q}$ the heat transfer to or from the system (kW), h the enthalpy of flow (kJ/kg), $\dot{E}_Q$ the exergy rate related to the heat transfer from or to the system, and e the

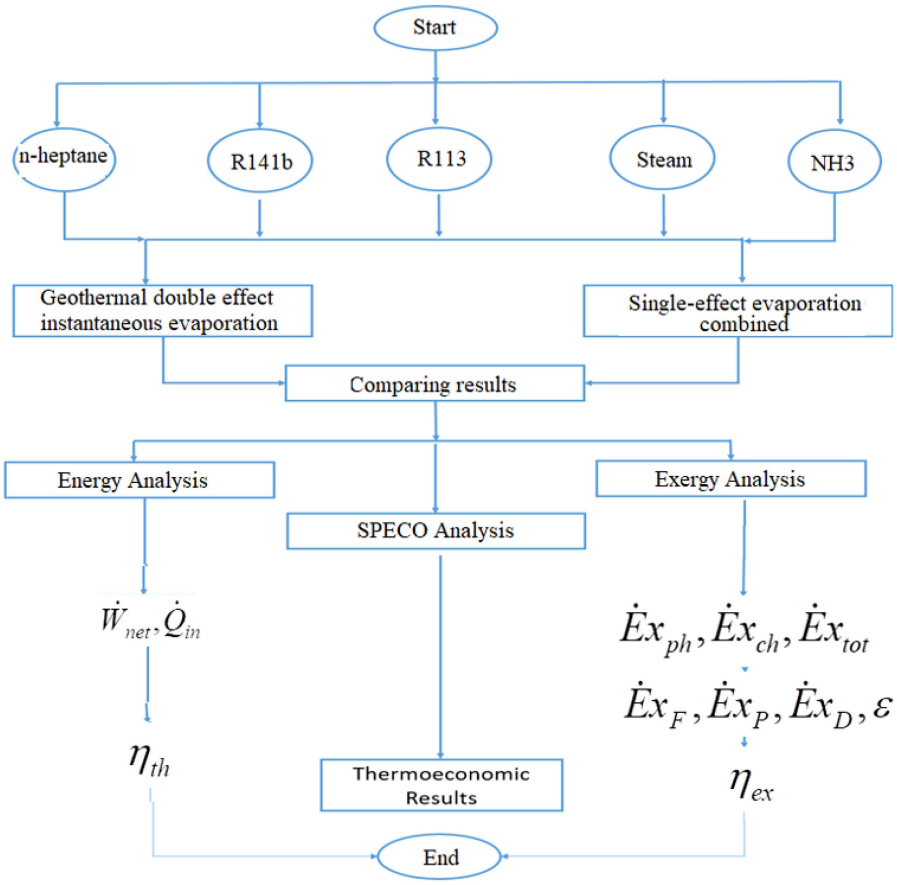

Figure 4. Flowchart of the procedure.

total specific exergy (kJ/kg). The specific exergy is proportional to the work that was done to transfer one kilogram of the system from its initial state to a state that is in mechanical and thermal equilibrium with the environment. Indices i and e are indicative of the input states to the control volume and its output, and $\dot{E}_D$ is the rate of exergy degradation (kW). Other sentences are evident in Eqs. (4)–(8):

$$\dot{E}_Q = \sum \left(1 - \frac{T_0}{T_i}\right) \dot{Q}_i, \tag{4}$$

$$\dot{E}_w = \sum \dot{W}, \tag{5}$$

$$\dot{E} = \dot{E}_{ph} + \dot{E}_{ch}, \tag{6}$$

$$\dot{E} = \dot{m}e, \tag{7}$$

$$e_{ph} = (h - h_0) - T_0(s - s_0), \tag{8}$$

where $\dot{E}_w$ is the exergy rate associated with power generation; $\dot{E}_{ph}$ and $\dot{E}_{ch}$ are the physical and chemical exergies of various currents in the system, respectively; and $\dot{E}$ is the total exergy of each current. The chemical exergy of a gaseous mixture is acquired from Eq. (9):

$$e_{ch}^{\text{mix}} = \sum_{i=1}^{n} x_i(e_{chi}) + RT_0 \sum_{i=1}^{n} x_i(Lnx_i), \tag{9}$$

where x_i is the molar ratio of the mixed components, and e_{chi} the chemical exergy of each component. In addition, e_{ch}^{mix} is also equivalent to the chemical exergy for the gas mixture.

2.1. Thermoeconomic analysis

In this study, the energy in the geothermal fluid was used to generate power. To this end, two power generation cycles were investigated using the geothermal fluid. The first cycle is the geothermal double-effect evaporation cycle, as shown in Figure 5. The second cycle analyzed in this study is the geothermal single-effect evaporation combined cycle and Rankine cycle with different organic fluids, the design of which is shown in Figure 6.

Engineering Equation Solver (EES) software performs the simulation and analysis of energy, exergy, and exergoeconomics [27,28]. In the EES software, there are internal functions that use these functions to obtain the physical characteristics of the geothermal fluid including enthalpy, entropy, specific volume, etc., anywhere. Initially, we examine the geothermal double-effect instantaneous evaporation cycle. The geothermal

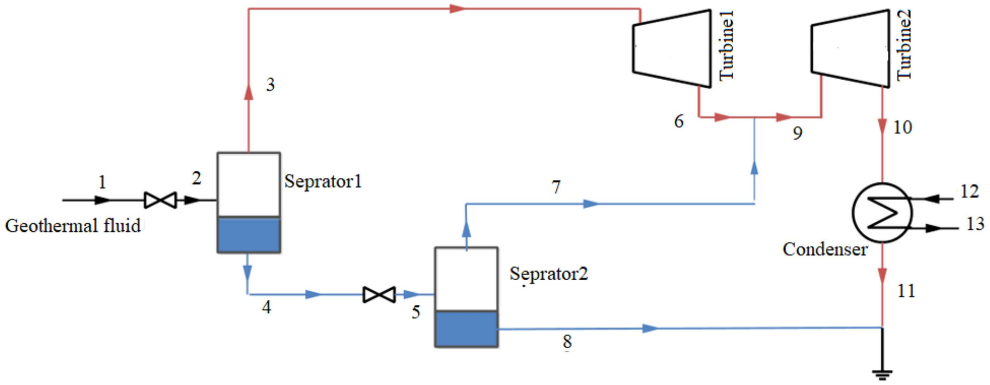

Figure 5. Schematic of the geothermal double-effect instantaneous evaporation cycle.

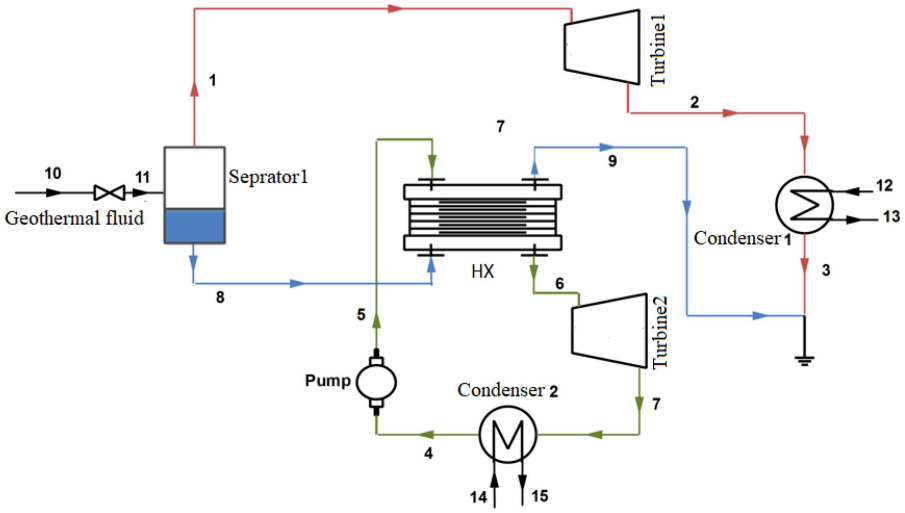

Figure 6. Schematic of the geothermal single-effect evaporation combined cycle.

fluid enters the cycle at a certain temperature, and its physical properties are obtained using the internal functions of EES. The following relations are considered in passing the geothermal fluid through the first trap valve (Eqs. (10) and (11)):

$$h_1 = h_2, \tag{10}$$

$$\dot{E}x_{D,TV1} = \dot{E}x_1 - \dot{E}x_2. \tag{11}$$

The geothermal fluid then passes through the first separator, and the geothermal fluid is converted into two parts, saturated liquid and saturated vapor. Exergy degradation in the first separator is obtained from Eq. (12):

$$\dot{E}x_{D,sep1} = \dot{E}x_2 - \dot{E}x_3 - \dot{E}x_4. \tag{12}$$

The saturated vapor of the geothermal fluid enters the first turbine. Once the isentropic efficiency is defined for a turbine, Eq. (13) can be obtained as:

$$\eta_T = \frac{h_3 - h_6}{h_3 - h_{6,5}}, \tag{13}$$

where $h_{6,s}$ is the output enthalpy of the first turbine in a state where the input and output entropies of the first turbine are equal. Here, h_6 is used to determine the temperature of the exhaust gases from the turbine. The output pressure of the first turbine is equal to the pressure of the second separator. The power output of the first turbine is obtained from Eq. (14):

$$\dot{W}_{T1} = \dot{m}_3(h_3 - h_6). \tag{14}$$

The exergy degradation of the first turbine is calculated via Eq. (15):

$$\dot{E}x_{D,T1} = \dot{E}x_3 - \dot{W}_{T1} - \dot{E}x_6. \tag{15}$$

The saturated liquid of the first separator output also reaches the second separator pressure by passing through the second trap valve. Thus, we have two equations, as given below (Eqs. (16) and (17)):

$$h_4 = h_5, \tag{16}$$

$$\dot{E}x_{D,TV2} = \dot{E}x_4 - \dot{E}x_5. \tag{17}$$

Further, exergy degradation in the second separator can be obtained from Eq. (18):

$$\dot{E}x_{D,sep2} = \dot{E}x_5 - \dot{E}x_7 - \dot{E}x_8. \quad (18)$$

The saturated vapor portion of the geothermal fluid output from the first separator is mixed with the output of the first turbine and then, it enters the second turbine. In the second turbine, we have Eq. (19):

$$\eta_T = \frac{h_9 - h_{10}}{h_9 - h_{10,5}}, \quad (19)$$

where $h_{10,s}$ is the output enthalpy of the second turbine in a state where the input and output entropies of the second turbine are equal. Based on h_{10}, the temperature of the output gases from the second turbine can be measured. The power output of the second turbine is acquired from Eq. (20):

$$\dot{W}_{T2} = \dot{m}_9(h_9 - h_{10}). \quad (20)$$

The exergy degradation of the second turbine is achieved from Eq. (21):

$$\dot{E}x_{D,T2} = \dot{E}x_9 - \dot{W}_{T2} - \dot{E}x_{10}. \quad (21)$$

The fluid output from the second turbine enters the condenser. The energy and exergy relations for the condenser are as follows (Eqs. (22) and (23)):

$$\dot{m}_{10}(h_{10} - h_{11}) = \dot{m}_{12}(h_{13} - h_{12}), \quad (22)$$

$$\dot{E}x_{D,cond} = \dot{E}x_{109} - \dot{W}_{x12} - \dot{E}x_{11} - \dot{E}x_{13}. \quad (23)$$

The total net power of the geothermal double-effect instantaneous evaporation cycle is obtained from Eq. (24):

$$\dot{W}_{net} = \dot{W}_{T1} + \dot{W}_{T2}. \quad (24)$$

Geothermal single-effect evaporation combined cycle and Rankine cycle are then examined. The geothermal fluid enters the cycle at a certain temperature, and its physical properties are obtained using the internal functions of EES. With regard to the passage of the geothermal fluid through the first trap valve, we will have Eqs. (25) and (26):

$$h_{10} = h_{11}, \quad (25)$$

$$\dot{E}x_{D,TV1} = \dot{E}x_{10} - \dot{E}x_{11}. \quad (26)$$

The geothermal fluid then passes through the first separator, and the geothermal fluid is converted into two parts of saturated liquid and saturated vapor. Exergy degradation in the first separator is obtained from Eq. (27):

$$\dot{E}x_{D,sep1} = \dot{E}x_{11} - \dot{E}x_1 - \dot{E}x_8. \quad (27)$$

Subsequently, the saturated vapor part of the geothermal fluid enters the geothermal fluid turbine. Through defining the isentropic efficiency for the first turbine, we will have Eq. (28):

$$\eta_T = \frac{h_1 - h_2}{h_1 - h_{2,5}}, \quad (28)$$

where $h_{2,s}$ is the output enthalpy of the geothermal turbine in a state where the input and output entropies of the geothermal turbine are equal. Based on h_2, the temperature of the output gases from the turbine is calculated. The power output of a geothermal turbine is obtained from Eq. (29):

$$\dot{W}_{T1} = \dot{m}_1(h_1 - h_2). \quad (29)$$

The exergy degradation of a geothermal turbine is determined via Eq. (30):

$$\dot{E}x_{D,T1} = \dot{E}x_1 - \dot{W}_{T1} - \dot{E}x_2. \quad (30)$$

The output fluid from the geothermal turbine enters the first condenser. The energy and exergy relationships for the first condenser are as follows (Eqs. (31) and (32)):

$$\dot{m}_2(h_2 - h_3) = \dot{m}_{12}(h_{13} - h_{12}), \quad (31)$$

$$\dot{E}x_{D,cond1} = \dot{E}x_2 - \dot{E}_{x12} - \dot{E}x_3 - \dot{E}x_{13}. \quad (32)$$

The saturated liquid part of the output from the first separator enters a heat exchanger as a heat source for a Rankine power generation cycle with organic operating fluid. The relations of the energy and exergy in the converter are given below (Eqs. (33) and (34)):

$$\dot{m}_8(h_8 - h_9) = \dot{m}_5(h_6 - h_5), \quad (33)$$

$$\dot{E}x_{D,HX} = \dot{E}x_8 - \dot{E}_{x5} - \dot{E}x_9 - \dot{E}x_6. \quad (34)$$

Next, the organic fluid enters the Rankine cycle turbine by absorbing heat from the saturated liquid part of the geothermal fluid. In the Rankine cycle turbine, we have Eq. (35):

$$\eta_T = \frac{h_6 - h_7}{h_6 - h_{7,5}}, \quad (35)$$

where $h_{7,s}$ is the output enthalpy of the Rankine cycle turbine as long as the input and output entropies of the cycle are equal. Based on h_7, the temperature of the output gases from the Rankine cycle turbine is obtained. In addition, the power output of the Rankine cycle turbine is obtained from Eq. (36):

$$\dot{W}_{T2} = \dot{m}_6(h_6 - h_7). \quad (36)$$

The exergy degradation of the Rankine cycle turbine is determined through Eq. (37):

$$\dot{E}x_{D,T2} = \dot{E}x_6 - \dot{W}_{T2} - \dot{E}x_7. \quad (37)$$

The output fluid from the Rankine cycle turbine enters

the second condenser. The relations of energy and exergy for the second capacitor are as follows (Eqs. (38) and (39)):

$$\dot{m}_7(h_7 - h_4) = \dot{m}_{14}(h_{15} - h_{14}), \tag{38}$$

$$\dot{E}x_{D,cond2} = \dot{E}x_7 - \dot{E}x_{14} - \dot{E}x_{15} - \dot{E}x_4. \tag{39}$$

The organic fluid output from the second condenser enters the pump to reach the pressure above the Rankine cycle [29–31]. The temperature of the fluid output from the pump is obtained from Eq. (40):

$$\frac{v_4(p_5 - p_4)}{\eta_p} = h_5 - h_4, \tag{40}$$

where v_4 is the specific volume of fluid at the pump inlet. The pump power required is obtained from Eq. (41):

$$\dot{W}_p = \dot{m}_4(h_5 - h_4). \tag{41}$$

In addition, the exergy degradation of the pump is equal to Eq. (42):

$$\dot{E}x_{D,P} = \dot{E}x_4 - \dot{W}_p - \dot{E}x_5. \tag{42}$$

The total net power of the geothermal single-effect evaporation combined cycle and Rankine cycle is obtained from Eq. (43):

$$\dot{W}_{net} = \dot{W}_{T1} + \dot{W}_{T2} - \dot{W}_p. \tag{43}$$

2.2. Exergoeconomic analysis

Multiple methods and strategies have been proposed in scientific sources for exergoeconomic analysis. This study employs the Specific Exergy Costing (SPECO) method which is on the basis of exergy, exergy efficiency, and auxiliary equations for heating system components and involves the following three steps [32–34]:

1. Identification of exergy currents;
2. Definition of fuel and product for each system component;
3. Allocation of cost equations.

The product shows the desired results of a component or system, and the fuel indicates the resources used to produce the product. Of note, it is not necessarily a real fuel such as natural gas, diesel fuel, etc. [35–40]. Fuel and product are both expressed in terms of exergy and for each system component. The third step in the analysis is to write cost equations. In this step, a parameter called the current cost rate C [$/s] is defined for each exergy current in the system [41]. The equilibrium price equation for each component of the system that gets heat and performs work is as follows (Eq. (44)):

$$\sum_e \dot{C}_{e,k} + \dot{C}_{w,k} = \dot{C}_{q,k} + \sum_i \dot{C}_{i,k} + \dot{Z}_k, \tag{44}$$

where $\dot{Z}_k$ is the initial cost rate of component k; i and e indices represent the input and output flows, respectively; and $\dot{C}_{q,k}$ and $\dot{C}_{w,k}$[$/s] represent the costs associated with heat transfer and work, respectively. Hence, when one of the components of the system such as the compressor is desired, the second sentence of the first side of the equation can be moved to the right of the equation with a positive sign.

$\dot{C}_{w,k}$ is obtained from the relation $\dot{C}_{w,k} = c_w\dot{W}$. In addition, upon multiplying the values of c_w and $\dot{W}$ for the turbine, the value for the parameter $\dot{C}_{w,k}$ can be obtained. We have $\dot{C}_{q,k} = c_q\dot{Q}$ where $\dot{Q}$ stands for the heat transfer to the environment. Since the amount of heat transfer to the environment in this study is considerably low while the amount of heat transfer is neglected in some components such as turbines [42–44], the value of the parameter $\dot{C}_{q,k}$ is overlooked in most components of the cycle. The cycles under study were modeled using EES software. Table 1 depicts the input parameters of the cycles.

3. Results

3.1. Validation

Table 2 presents the obtained results in [45] at the initial temperature of 162°C. However, in this study, the initial temperature was considered as 175°C. Hence, the initial parameters of the study were used for a cycle to yield the following results.

3.2. Numerical results

As observed in Figure 7, the results obtained under similar conditions for the present study and Ref. [45] are quite close and in the worst case, the difference between results is less than 2%. For this reason, the analysis method proposed in this research was acceptable and adequate. Then, the parameters of the different cycles affecting the energy, exergy, and exergoeconomic performance of these cycles were examined, and the effects of changes in these parameters in a certain range on the performance of systems were analyzed.

As shown in Figure 7, at a constant value of 110 kPa for the second separator, increasing the pressure of the first separator reduces the energy efficiency and exergy. However, the exergy loss in the double-effect instantaneous evaporation cycle decreases. The exergetic performance coefficient, which is similar to the efficiency coefficient, decreases as the pressure of the first separator increases. The power output of the first turbine at the pressure of 350 kPa for the first separator reaches its highest value and, then, decreases. However, both power output of the second turbine and total net output power of the cycle decrease as the

Table 1. Input parameters of cycles.

Parameter	Parameters	Input	Unit
Input geothermal fluid temperature to the cycles	T_i	175	°C
Mass flow rate of input geothermal fluid temperature to the cycles	$\dot{m}_i$	100	kg/s
Input pressure of first separator	$P_{i,2}$	320	kPa
Isentropic efficiency of turbines	η_T	80	%
Isentropic efficiency of pump	η_p	85	%
Output temperature of Rankine cycle condenser	T_4	40	°C
Temperature of the two-phase part in the Rankine cycle's heat exchanger	T_{ev}	115	°C
Temperature difference between points 8 and 6 in the combined cycle	$T_8 - T_6$	10	°C
Turbine 1 output pressure in the combined cycle	P_2	30	kPa
The second separator pressure in the double-effect instantaneous evaporation cycle	P_5	110	kPa
Condenser pressure in the double-effect instantaneous evaporation cycle	P_{11}	30	kPa
Input water temperature to condensers	T_{12} & T_{14}	25	°C
Input water pressure to condensers	P_{12} & P_{14}	100	kPa
Maintenance coefficient of cycle components	φ	6	%
Interest rate	I	10	%
Inflation rate	i_r	5	%
System service life	n	20	Year
System operation hours per year	N	7446	Hour

Table 2. Comparison of the results with those in [37].

Points	Reference results [37] for enthalpy	Research results for enthalpy	Reference results [37] for pressure	Research results for pressure	Reference results [37] temperature	Research results for temperature
1	684.2	684.4	650.3	650.3	162	162
2	684.2	684.4	205.3	205.3	121	121
3	2707	2708	205.3	205.3	121	121
4	–	508.25	–	205.3	–	121
5	508.2	508.25	52.6	52.6	82.6	82.58
6	–	2540	–	52.6	–	82.58
7	2647	2647	52.6	52.6	82.6	82.58
8	–	345.8	–	52.6	–	82.58
9	–	2588	–	52.6	–	82.58
10	2374	2408	10	10	45.8	45.76
11	191.8	191.7	10	10	45.8	45.79
12	75.5	75.5	2.1	2.1	18	18
13	117.4	116.9	3.8	3.8	28	27.6

pressure of the first separator increases. As observed, the costs of power generation and exergy degradation increase as the condenser pressure increases while the value of the exergoeconomic parameter f decreases. The cost of purchasing and maintaining components at a pressure of 350 kPa, i.e., the pressure at which Turbine 2 produces the utmost power, reaches its highest value and consequently, the total costs of exergy degradation and component purchases decrease as the first separator pressure increases.

According to Figure 8, upon increasing the pressure of the first separator, the mass flow rate passing through the first turbine undergoes a constant decrease. However, it was observed that upon increasing the pressure of the first separator, the temperature and enthalpy of the input flow to the turbine (T [3] & h [3])

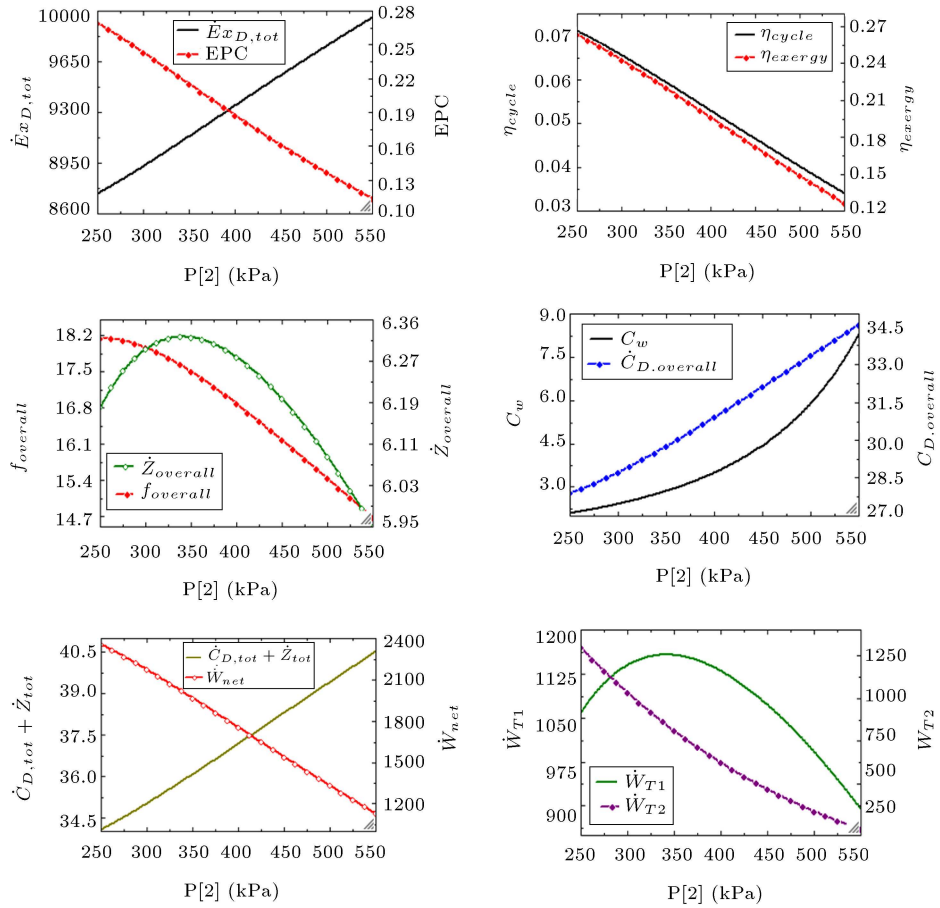

Figure 7. The effect of variations in the first separator pressure on the performance of the double-effect instantaneous evaporation cycle.

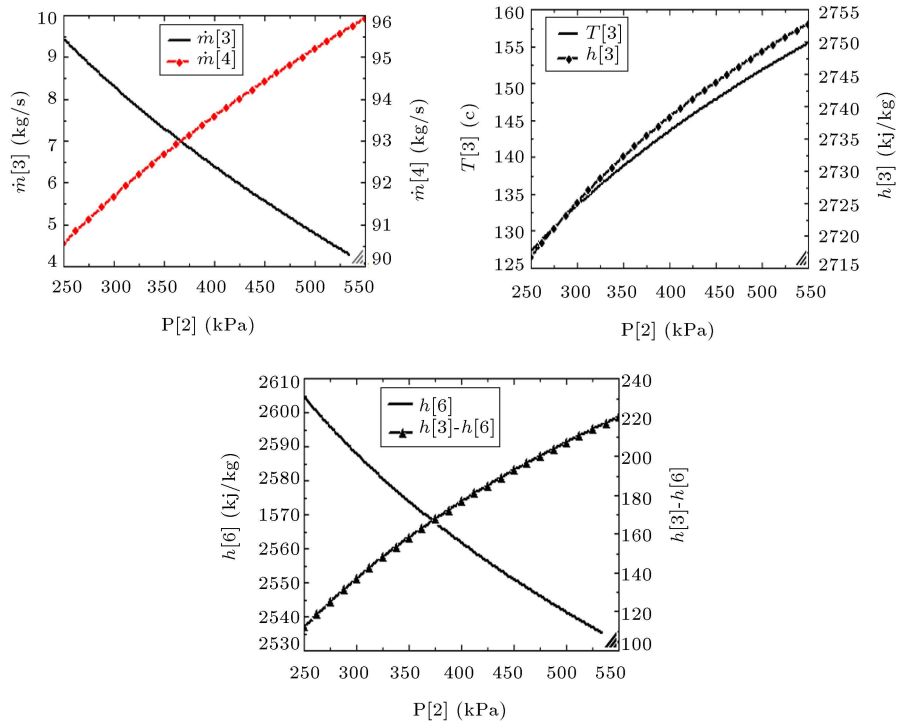

Figure 8. Mass flow rate and temperature curves of points 3 and 4.

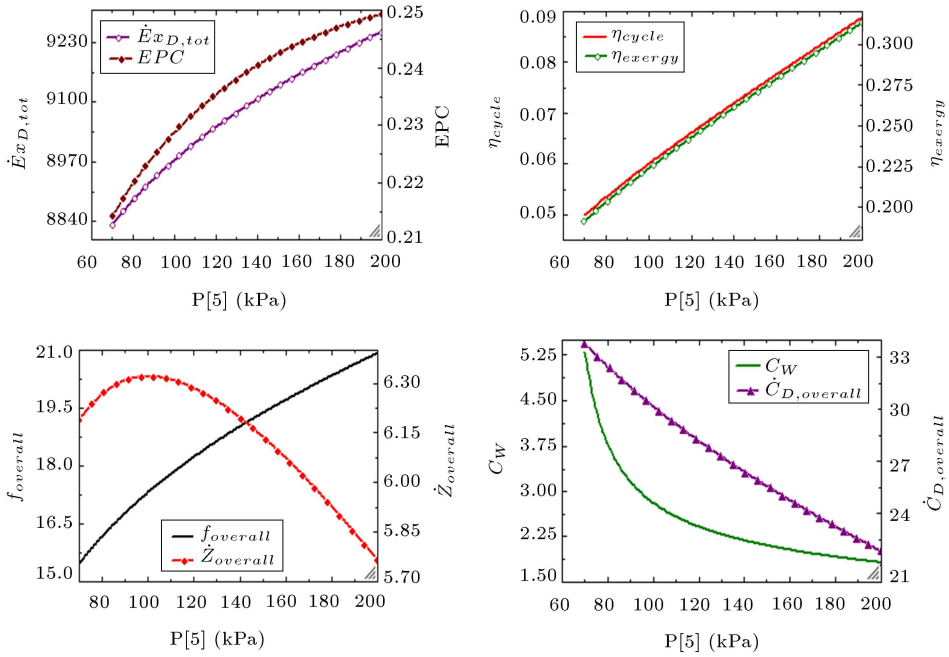

Figure 9. Impact of the second separator pressure variations on the performance of the double-effect instantaneous evaporation cycle.

increased, and the total value of h [3] -h [6] continuously rose. According to the relationship of the turbine power m [3]*(h [3] -h [6]), first, the incremental slope of h [3] -h [6] overcomes the slope m [3], hence an increase in the output power of Turbine 1. However, at higher pressures of the first separator, the decreasing slope of m [3] overcomes the increasing slope of h [3] -h [6], hence a decrease in the output power of Turbine 1. In this regard, the power generation diagram of Turbine 1 shows the maximum point (peak).

Based on Figure 9, it can be inferred that at a constant pressure of 320 kPa for the first separator and increasing the pressure for the second one, the efficiency of the first and second laws as well as and the exergy performance coefficient increase. It was also observed that upon increasing the pressure of the second separator, the rate of exergy degradation would increase. On the contrary, the power output of the first turbine decreased by increasing the pressure of the first separator, while the power output of the second turbine increased. Overall, the effect of the behavior of the first turbine is dominant and the total net generated power of the double-effect instantaneous evaporation cycle increased by increasing the pressure in the second separator.

According to the observations, at a constant pressure of the first separator, as the pressure of the second separator increased, the costs of the power output and exergy degradation decreased, contrary to the behavior of the exergy degradation rate. In general, according to the definition of the exoeconomic parameter f and given the reduction in the exergy degradation cost, the parameter f increased with an increase in the pressure of the second separator. Further, it was observed that the cost of purchasing and maintaining cycle components at the constant pressure of the first separator reached its maximum value at the pressure of roughly 100 kPa for the second separator and, then, decreased. Nonetheless, with an increase in the second separator pressure, the cost associated with exergy degradation exceeded the purchase and maintenance costs. In general, the parameters $\dot{C}D$, k, $k + \dot{Z}_k$ will decrease as the second separator pressure increases.

In Figure 10, followed by increasing the separator pressure in the combined cycles, the efficiency of the first and second laws, exergy performance coefficient, and net productive power of the combined cycles increase while the rate of destruction exergy decreases. As observed, the highest slope is attributed to the ammonia operating fluid, while the lowest one to the n-heptane and R113. Among the combined cycles studied, the combined cycle with n-heptane operating fluid has the lowest efficiency and power output. Of note, up to the separator pressure of 430 kPa, the efficiency and power output of a combined cycle with R141b are higher than that those of a combined cycle with ammonia. However, at higher pressures, the efficiency and power output of the ammonia cycle will be higher than those of the R141b cycle.

Figure 11 indicates that increasing the separator pressure at a constant evaporator temperature will decrease the power generation cost for all combined cycles with the operating fluids. The lowest and highest power generation costs are attributed to the combined

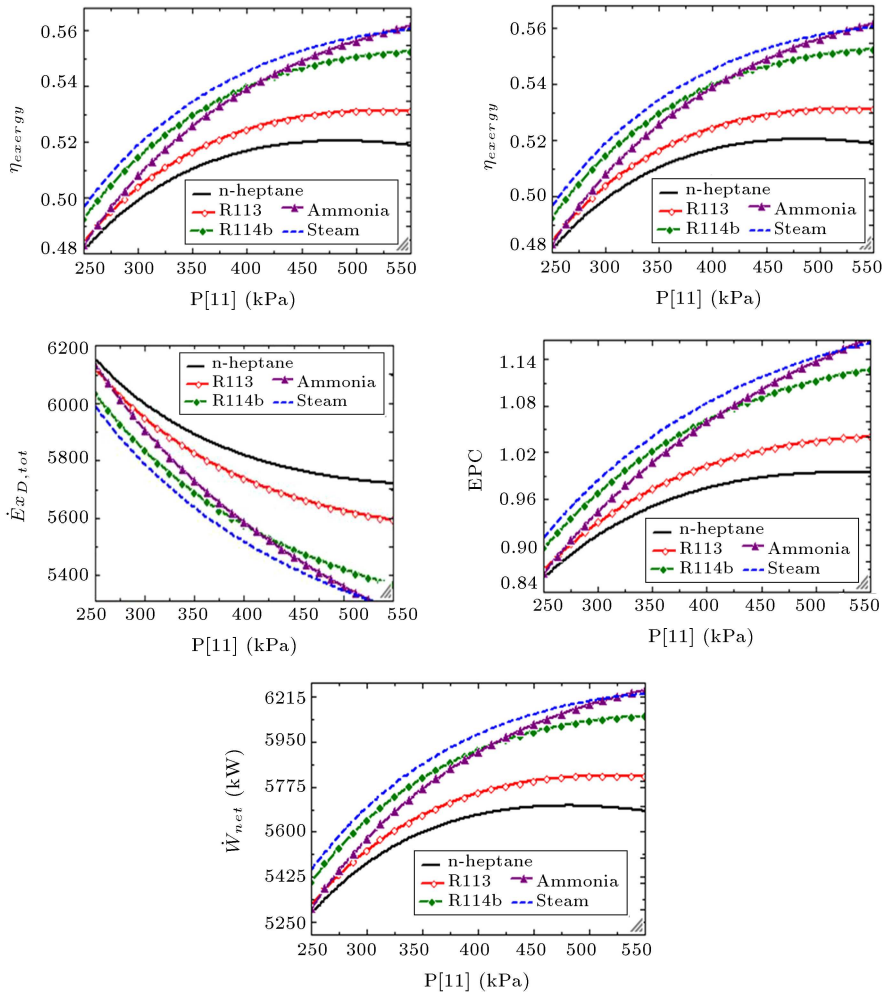

Figure 10. The effect of the separator pressure variations on the performance of the combined cycles.

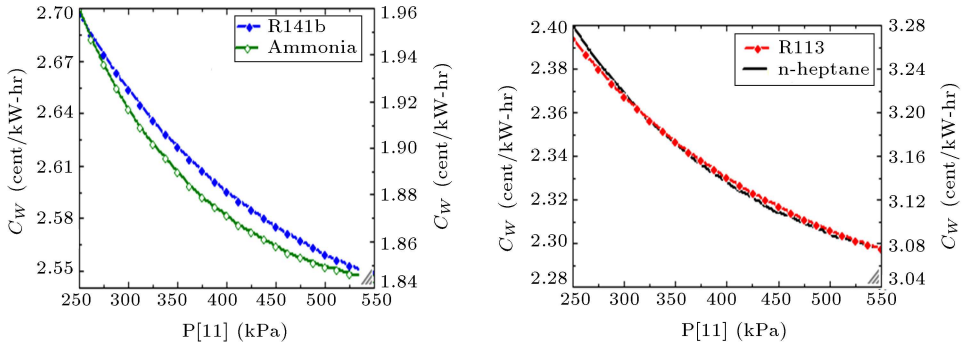

Figure 11. The effect of the pressure variations on the efficiency of the first and second laws and the net power output of the combined cycles.

cycle with the operating fluid R113 and combined cycle with the ammonia operating fluid, respectively. Based on the figures below, the cost associated with exergy degradation decreases upon increasing the separator pressure. In addition, the slope is the highest for ammonia and the lowest for n-heptane.

As the separator pressure increases in the combined cycle, the value of the exoeconomic parameter f increases for all combined cycles with different operating fluids. This finding could be predicted by reducing the cost of exergy degradation through an increase in the separator pressure and exergoeconomic parameter definition.

As observed in Figures 12–14, the parameter D, $k + \dot{Z}_k$ increases for the combined cycles with different operating fluids as the separating pressure increases.

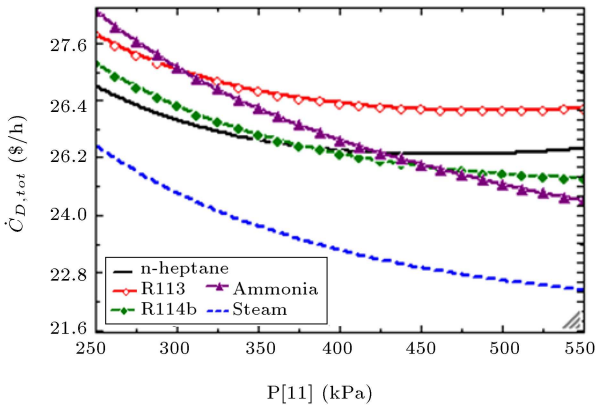

Figure 12. Impact of the pressure variations on the power generation cost for different fluids.

However, in the case of ammonia and water vapor operating fluids, this parameter first decreases and, then, follows an upward trend, implying that at low separator pressures, the effect of exergy degradation cost is dominant that in turn causes a reduction in the parameter $\dot{C}D$, $k + \dot{Z}_k$. Nonetheless, at higher separator pressures, the cost of purchase and maintenance of components causes an increase in the value of the parameter $\dot{C}D$, $k + \dot{Z}_k$.

As observed from Figure 15, at a constant pressure of 320 kPa for the separator, the efficiency of the first and second laws of the combined cycles with the different operating fluids under test increases as the temperature of the evaporator rises. Here, the maximum and minimum efficiencies of the first and second laws are attributed to the combined cycle with water vapor and the combined cycle with n-heptane, respectively. In addition, it can be inferred from the figures that the behavior of the exergy performance coefficient and net power output is the same as that of the thermodynamic efficiencies. Upon increasing the evaporator pressure, the rate of exergy degradation for the combined cycles decreases and the combined cycle with the water vapor-operating fluid shows the highest decrease in the mentioned rate. The highest efficiency of the first and second laws is attributed to the single-effect evaporation combined cycle and Rankine cycle with water vapor operating fluid. The combined cycles with the operating fluids of R141b, ammonia, R113, and n-heptane are ranked next. The lowest efficiency of the first and second laws is related to the geothermal double-effect instantaneous evaporation cycle. The efficiency of the combined cycle with R141b is higher than that of the combined cycle with ammonia. The cost of power generation in the combined cycle with ammonia is lower than that in the combined cycle with R141b.

In the double-effect instantaneous evaporation cycle, condenser and Turbine 2 hold the highest value of this parameter, respectively. In combined cycles with different operating fluids, both Turbine 2 and condensers hold the highest value of this parameter. Consequently, these components are of utmost importance from the exoeconomic perspective. Special

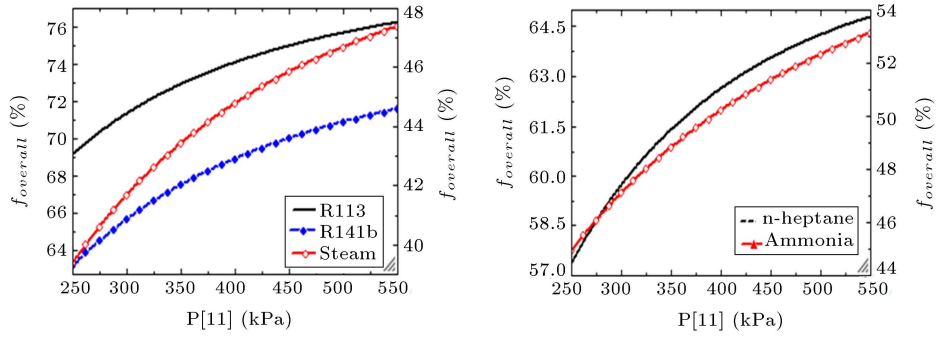

Figure 13. The impact of the pressure variations on the exergy degradation cost.

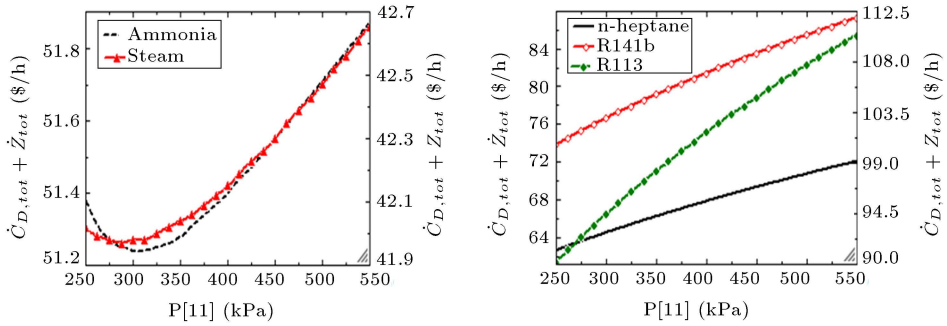

Figure 14. The effect of the pressure variations on the parameter D, $k + \dot{Z}_k$.

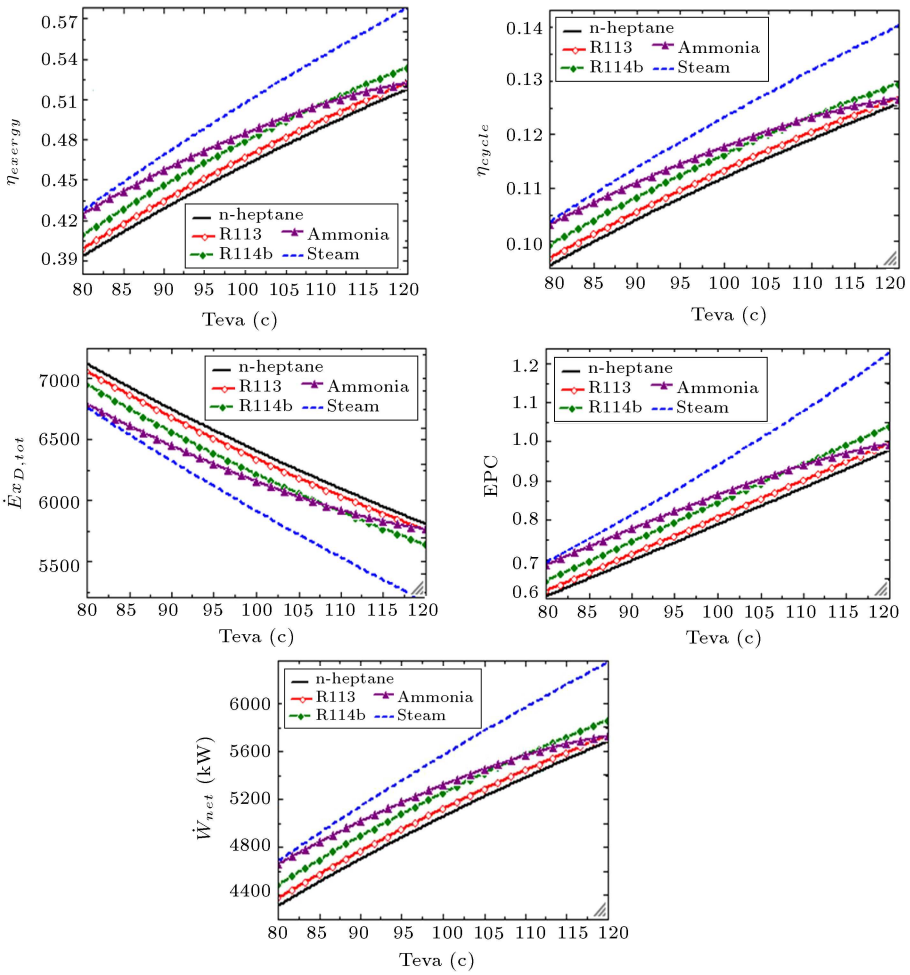

Figure 15. The effect of the evaporator temperature variations on the performance of the combined cycles.

attention should be paid to these components to enhance the exoeconomic performance of the examined cycles.

The values of the exoeconomic parameter (f) for the separator, trap valve, and condensers are relatively small, indicating that the cost associated with exergy degradation is significantly greater than that of purchasing and maintaining components.

In a double-effect instantaneous evaporation cycle, increasing the first separator pressure reduces the energy efficiency and exergy and, consequently, decreases the exergy losses of the cycle.

In a double-effect instantaneous evaporation cycle, the costs of power generation and exergy degradation increase by increasing the pressure of the first separator. However, the value of the exoeconomic parameter f decreases. The cost of purchasing and maintaining components at the pressure of 350 kPa, i.e., the pressure at which Turbine 2 produces the utmost power, has the maximum value.

In the double-effect instantaneous evaporation cycle, at the constant pressure of the first separator, as the pressure of the second separator increases, the costs of the power output and exergy degradation would decrease, contrary to the behavior of the exergy degradation rate.

In a double-effect instantaneous evaporation cycle, the cost of purchasing and maintaining cycle components at the constant pressure of the first separator reaches its maximum value at the pressure of approximately 100 kPa in the second separator and, then, is reduced. Overall, the cost effect associated with exergy degradation overcomes the cost behavior of component purchase and maintenance. The parameters $\dot{C}_{D,k,k} + \dot{Z}_k$ are generally reduced upon increasing the pressure of the second separator.

Based on Figure 16, power generation cost undergoes changes in the combined cycles with evaporator temperature. Here, upon increasing the evaporator temperature, combined cycles reach their minimum values while the optimal evaporator temperatures for combined cycles with different operating fluids are different. For example, in a combined cycle with the ammonia operating fluid, the optimum evaporator temperature is 110°C and the power generation cost

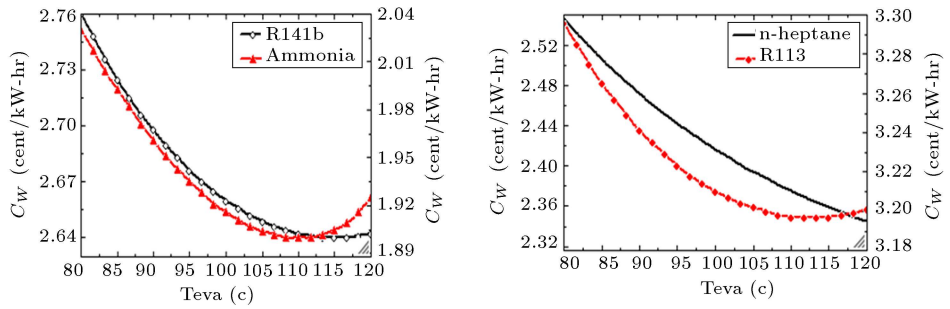

Figure 16. The effect of evaporator temperature changes on the generation cost.

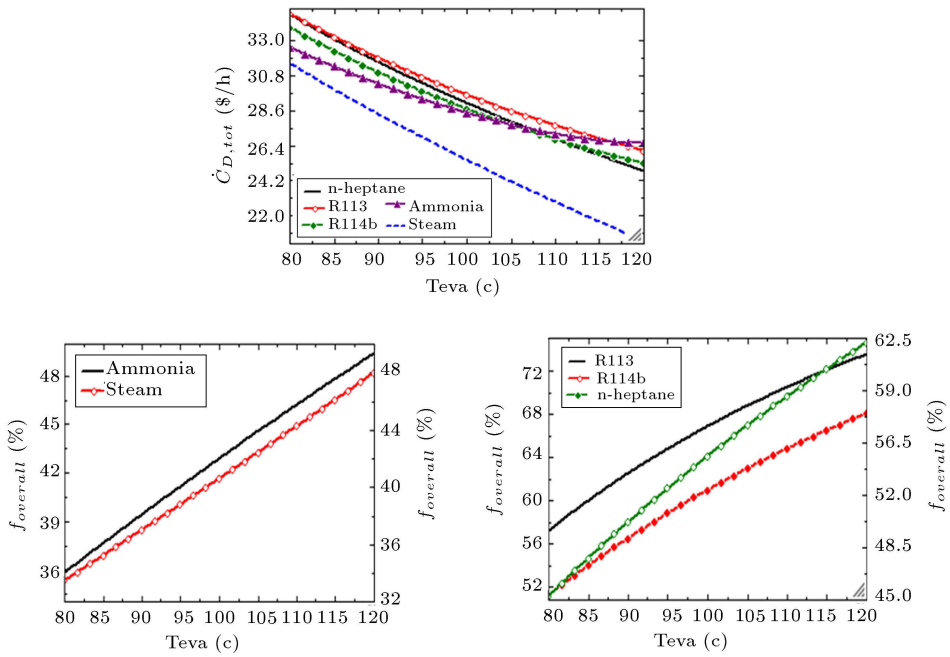

Figure 17. The effect of evaporator temperature changes on the cost of exergy degradation.

at this temperature is 2.63 cent/kW-hr. In contrast, in a combined cycle with the R141b operating fluid, this optimal temperature is equal to 115°C, and the cost of power generation at this temperature is equal to 2.64 cent/kW-hr. Of note, increasing the evaporator temperature will reduce the cost associated with exergy degradation. The combined cycle with water vapor and combined cycle with R113 has the lowest and highest values, respectively.

According to Figure 17, followed by decreasing the cost of exergy degradation by increasing separator pressure and according to the definition of exoeconomic parameter f, upon increasing the separator pressure in the combined cycle, the values for the exergoeconomic parameter in all combined cycles with different operating fluids would increase.

In the combined cycles, at a separation pressure of up to 430 kPa, the efficiency and power output of the combined cycle with R141b are higher than those of the combined cycle with ammonia. However, at higher pressures, the efficiency and power output of the ammonia cycle will be greater than for the R141b cycle. Increasing the separator pressure at the constant evaporator temperature will reduce the power generation cost for all combined cycles with the operating fluids. The lowest power generation cost is related to the combined cycle with the operating fluid R113. The highest amount of power generation cost is attributed to the combined cycle with the ammonia operating fluid.

In combined cycles, the value for the parameter $\dot{C}_{D,k} + \dot{Z}_k$ increases in the combined cycles with different operating fluids by increasing the separating pressure. On the contrary, in the case of ammonia and water vapor operating fluids, the value for this parameter first decreases and, then, increases. This implies that the effect of the exergy degradation cost is predominant at low separator pressures, and the parameter $\dot{C}_{D,k} + \dot{Z}_k$ is reduced. However, at higher separator pressures, the cost of purchasing and

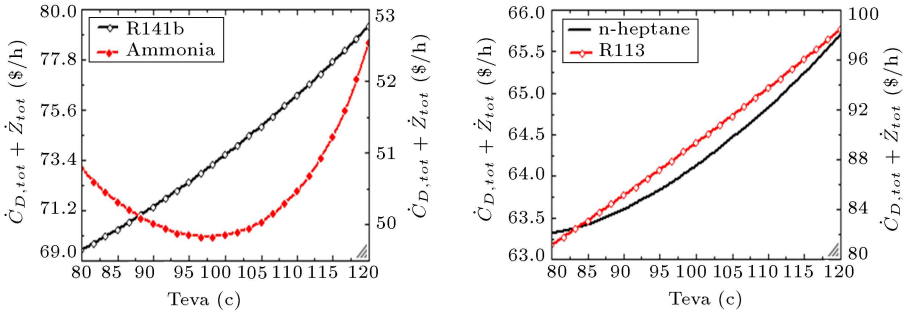

Figure 18. The effect of evaporator temperature changes on the parameter D, $k + \dot{Z}_k$.

maintaining the components increases the parameter $\dot{C}_{D,k} + \dot{Z}_k$.

As shown in Figure 18, by increasing the evaporator temperature, the values for the parameters $\dot{C}_{D,k} + \dot{Z}_k$ in the combined cycles with different operating fluids, except for ammonia, follow a completely upward trend. However, in the combined cycle with ammonia, this parameter first decreases, reaches its minimum value, and then increases at a higher evaporator temperature. In this combined cycle, the lowest value of the parameter $\dot{C}_{D,k}+\dot{Z}_k$ is obtained at a temperature of approximately 97°C. Therefore, it can be inferred that followed by increasing the evaporator temperature, the increasing behavior of the cost of the purchase and maintenance of cycle components overcomes the decreasing behavior of the cost associated with exergy degradation and causes the parameter $\dot{C}_{D,k} + \dot{Z}_k$ to increase with an increase in the evaporator temperature.

4. Conclusion

The current study investigated the geothermal double-effect instantaneous evaporation cycle, single-effect evaporation combined cycle, and Rankine cycle with different operating fluids in terms of energy and exergy. To this end, a thorough exergoeconomic analysis on the mentioned cycles was carried out, and different cycles were compared. In addition, a parametric study was carried out on the mentioned cycles, and the effect of changes in the functional parameters of the cycles on the thermodynamic and exergoeconomic performance of the cycles was analyzed and dissected. The significant findings of this study are summarized in the following:

√ The thermodynamic efficiency of a double-effect instantaneous evaporation cycle was significantly lower than that of a combined cycle with R141b. Having said that, its power generation cost was lower than that of the combined cycle with R141b, indicating that higher efficiency cycles could not necessarily ensure lower power generation costs;

√ The exergoeconomic coefficient, i.e., the ratio of the cost of purchasing components to the costs of the total exergy degradation and purchasing cycle components, reached its highest value in the case of combined cycle with R113 and its lowest value in the case of the double-effect instantaneous evaporation cycle;

√ In combined cycles, upon increasing the separator pressure, the efficiency of the first and second laws, coefficient of exergy performance, and net power output of the combined cycles increased, while the rate of exergy degradation decreased. Of note, the slope varied in different fluids. The highest slope was attributed to the ammonia operating fluid, and the lowest slope to the n-heptane and R113;

√ Combined cycles reached their minimum values by increasing evaporator temperature while the optimal evaporator temperature for combined cycles with different operating fluids was different. In addition, the cost associated with exergy degradation followed a downward trend upon increasing the evaporator temperature. The minimum value was attributed to the combined cycle with water vapor while the maximum value to the combined cycle with R113;

√ With an increase in the separated pressure, the value for the parameter $\dot{C}_{D,k} + \dot{Z}_k$ in combined cycles with different operating fluids, except for ammonia, followed an upward trend. Despite this, in the combined cycle with ammonia, first, this parameter decreased and reached a minimum value and, then, went up with a further increase in evaporator temperature.

Nomenclature

Symbols

A	Area (m^2)
abs	Absorber
bt	Binary turbine
Cp	Specific heat (J/kg.K)

D	Diameter (m)
D_O	Collector tube outlet diameter (m)
$e.v$	Expansion valve
e	Specific exergy (kJ/kg), evaporator
$\dot{E}$	Exergy rate (kW)
$\dot{E}_D$	Exergy destruction rate (kW)
h	Specific enthalpy (kJ/kg)
I_b	Beam irradiance (W.m^{-3})
K	Component
$\dot{m}$	Mass flow rate (kg/s)
M	Molecular mass (kg/kmol)
n	Number of solar collectors, day number
P	Pressure (bar), pump
Q	Heat transfer (kJ)
$\dot{Q}$	Heat transfer rate (kW)
$\dot{Q}_u$	Useful heat gain
S	Absorbed heat (kW)
s	Specific entropy (kJ/kg.K)
T	Temperature/turbine (°C)
T_r	Wall temperature
t	Day time
U	Overall heat transfer coefficient (kW/m^{2}K)
w_a	Aperture width (m)
W	Work (kJ)
$\dot{W}$	Power (kW)
Y_d	Exergy destruction ratio (%)
η_{cycle}	The efficiency of the first law
η_{exergy}	The efficiency of the second law
$\dot{E}_{D,tot}$	Total cycle exergy losses (kW)
$c_{w,T1}$	Turbine power generation cost 1 (cent/kW/hr)
f	Exercioeconomic coefficient of the whole cycle (%)
$\dot{W}_{T1}$	Turbine output power 1 (kW)
$\dot{W}_{T2}$	Turbine output power 2 (kW)
EPC	Total cycle exergy performance coefficient
$\dot{m}_{i,T}$	Turbine flow rate 1 (kg/s)
CI	Investment cost
OMC	Operation and Maintenance Cost
PT	Potential
KN	Kinetic

Greek symbols

η	Efficiency
ε	Exergetic efficiency
δ	Difference

Subscripts

F	Fuel
P	Product
D	Destruction
L	Loss
PP	Pinch Point
Aux	Auxiliary heater
i	Inlet
e	Exit
s	Isentropic
f	Saturated liquid
ref	Reference
CV	Control Volume
sat	Saturated
$Evap$	Evaporator
St	Steam turbine
HE	Heat Exchanger
P	Pump
gen	Generator
t	Time
$e.v$	Expansion valve
abs	Absorber
H_2O	Water
BT	Binary turbine
w	Power
q	Heat
0	Atmospheric condition

Abbreviations

Cond	Condenser
CCHP	Combined Cooling, Heat and Power
COP	Coefficient of Performance
EUF	Energy Utilization Factor
LHV	Lower Heating Value
HRSG	Heat Recovery Steam Generator
ORC	Organic Rankine Cycle
PVT	Photovoltaic-Thermal

References

1. Ahmadi, M.H., Baghban, A., Sadeghzadeh, M., et al. "Evaluation of electrical efficiency of photovoltaic thermal solar collector", *Engineering Applications of Computational Fluid Mechanics*, **14**(1), pp. 545–565 (2020).

2. Fan, G., Gao, Y., Ayed, H., et al. "Energy and exergy and economic (3E) analysis of a two-stage organic Rankine cycle for single flash geothermal power plant exhaust exergy recovery", *Case Studies in Thermal Engineering*, **28**, 101554 (2021).

3. Norouzi, N. "Thermodynamic and exergy analysis of cogeneration cycles of electricity and heat integrated with a solid oxide fuel cell unit", *Advanced Journal of Chemistry-Section A*, **4**(4), pp. 244–257 (2021).

4. Shamoushaki, M., Fiaschi, D., Manfrida, G., et al. "Energy, exergy, economic and environmental (4E) analyses of a geothermal power plant with NCGs reinjection", *Energy*, **244**, 122678 (2022).

5. Mirzaei, M., Ahmadi, M.H., Mobin, M., et al. "Energy, exergy and economics analysis of an ORC working with several fluids and utilizes smelting furnace gases as heat source", *Thermal Science and Engineering Progress*, **5**, pp. 230–237 (2018).

6. Ehyaei, M.A., Ahmadi, A., El Haj Assad, M., et al. "Investigation of an integrated system combining an organic Rankine cycle and absorption chiller driven by geothermal energy: Energy, exergy, and economic analyses and optimization", *Journal of Cleaner Production*, **258**, 120780 (2020).

7. Nourdanesh, N. and Ranjbar, F. "Investigation on heat transfer performance of a novel active method heat sink to maximize the efficiency of thermal energy storage systems", *Journal of Energy Storage*, **45**, 103779 (2022).

8. Yari, M. "Exergetic analysis of various types of geothermal power plants", *Renewable Energy*, **35**(1), pp. 112–121 (2010).

9. DiPippo, R. "Second law assessment of binary plants generating power from low-temperature geothermal fluids", *Geothermics*, **33**(5), pp. 565–586 (2004).

10. Walraven, D., Laenen, B., and D'haeseleer, W. "Comparison of thermodynamic cycles for power production from low-temperature geothermal heat sources", *Energy Conversion and Management*, **66**, pp. 220–233 (2013).

11. Jalilinasrabady, S., Itoi, R., Valdimarsson, P., et al. "Flash cycle optimization of Sabalan geothermal power plant employing exergy concept", *Geothermics*, **43**, pp. 75–82 (2012).

12. Liu, X., Wang, X., and Zhang, C. "Sensitivity analysis of system parameters on the performance of the organic rankine cycle system for binary-cycle geothermal power plants", *Applied Thermal Engineering*, **71**(1), pp. 175–183 (2014).

13. Mohammadi, B., Ranjbar, S.F., and Ajabshirchi, Y. "Comprehensive evaluation of a semi-solar greenhouse: Energy, exergy, and economic analyses with experimental validation", *Scientia Iranica*, **28**(5), pp. 2613–2627 (2021).

14. Liu, X., Sun, D., Qin, D., et al. "Multi-objective design optimization of power-cycling hydrodynamic mechanical transmissions", *Proceedings of the Institution of Mechanical Engineers, Part C: Journal of Mechanical Engineering Science*, **233**(4), pp. 1392–1410 (2019).

15. Wang, J., Wang, J., Dai, Y., et al. "Thermodynamic analysis and optimization of a transcritical CO2 geothermal power generation system based on the cold energy utilization of LNG", *Applied Thermal Engineering*, **70**(1), pp. 531–540 (2014).

16. Tempesti, D. and Fiaschi, D. "Thermo-economic assessment of a micro CHP system fuelled by geothermal and solar energy", *Energy*, **58**, pp. 45–51 (2013).

17. Zharfa, M. and Karimi, N. "Intensification of MILD combustion of methane and hydrogen blend by the application of a magnetic field-a numerical study", *Acta Astronautica*, **184**, pp. 259–268 (2021).

18. Athiyaman, A. and Magapa, T. "Market intelligence from the internet: An illustration using the biomass heating industry", *International Journal of Economics and Finance Studies*, **11**(1), pp. 1–6 (2019).

19. Zare Kazemabadi, F., Mirnezami, S.M.S., and Heydarinasab, A. "Using a two-dimensional finite element model to simulate biothermal transfer in the human eye) by considering the rate of tear evaporation and radiation to the eye surface", *Progress in Chemical and Biochemical Research*, **4**(3), pp. 305–318 (2021).

20. Zharfa, M., Hahsler, M., Olinick, E., et al. "Wake pattern identification using graph matching", *Bulletin of the American Physical Society*, **63**, pp. 56–65 (2018).

21. Krueger, P.S., Hahsler, M., Olinick, E.V., et al. "Quantitative classification of vortical flows based on topological features using graph matching", *Proceedings of the Royal Society A*, **475**(2228), 20180897 (2019).

22. Mohammadi, B., Ranjbar, S.F., and Ajabshirchi, Y. "Comprehensive evaluation of a semi-solar greenhouse: Energy, exergy, and economic analyses with experimental validation", *Scientia Iranica*, **28**(5), pp. 2613–2627 (2021).

23. Liu, F., Yang, C., Li, B., et al. "Thermodynamic and economic sensitivity analyses of a geothermal-based trigeneration system; performance enhancement through determining the best zeotropic working fluid", *Energy*, **246**, 123310 (2022).

24. Ahmadi, Z., Haghighi, M., and Validi, Z. "A novel approach for energy optimization in distributed databases in wireless network applications", *Journal of Management and Accounting Studies*, **8**(3), pp. 65–78 (2020).

25. Hajipour Khire Masjidi, B., Bahmani, S., Sharifi, F., et al. "CT-ML: Diagnosis of breast cancer based on ultrasound images and time-dependent feature extraction methods using contourlet transformation and machine learning", *Computational Intelligence and Neuroscience*, **24**, 1493847 (2022). DOI: 10.1155/2022/1493847

26. Okon E.O. "Consequence of environmental policy on the dynamics of economic growth and environmental degradation in Nigeria", *International Journal of Social Sciences and Humanity Studies*, **13**(1), pp. 195–217 (2021).

27. Attuluri, R., Dheer, D.K., and Tagore, Y.R. "A review on the progress of intermetallic solid-state hydrogen storage material for fuel cell vehicles", *European Chemical Bulletin*, **11**(1), pp. 17–29 (2022).

28. Li, T., Liu, Q., Gao, X., et al. "Thermodynamic, economic, and environmental performance comparison of typical geothermal power generation systems driven by hot dry rock", *Energy Reports*, **8**, pp. 2762–2777 (2022).

29. Bozorgian, A. "Analysis and simulating recuperator impact on the thermodynamic performance of the combined water-ammonia cycle", *Progress in Chemical and Biochemical Research*, **3**(2), pp. 169–179 (2020).

30. Salim, F.B., Shiaka, G.P., and Muhammad, M. "Influence of reaction temperature on bioethanol production by saccharomyces cerevisiae using cassava as substrate", *International Journal of Sustainable Energy and Environmental Research*, **10**(1), pp. 9–16 (2021).

31. Putra, A.B. "Computer technology simulation towards power generation potential from coproduced fluids in south lokichar oil fields", *International Journal of Communication and Computer Technologies*, **8**(2), pp. 9–12 (2020).

32. Olasehinde, E., Abegunde, S., and Adebayo, M. "Adsorption isotherms, kinetics and thermodynamic studies of methylene blue dye removal using Raphia taedigera seed activated carbon", *Caspian Journal of Environmental Sciences*, **18**(4), pp. 329–344 (2020).

33. Sibuea, M.B., Sibuea, S.R., and Pratama, I. "The impact of renewable energy and economic development on environmental quality of ASEAN countries", *AgBioForum*, **23**(1), pp. 12–21 (2021).

34. Band, S.S., Al-Shourbaji, I., Karami, et al. "Combination of group method of data handling (GMDH) and computational fluid dynamics (CFD) for prediction of velocity in channel intake", *Applied Sciences*, **10**(21), 7521 (2020).

35. Khorsandi, Z., Afshinpour, M., Molaei, F., et al. "Design and synthesis of novel phe-phe hydroxyethylene derivatives as potential coronavirus main protease inhibitors", *Journal of Biomolecular Structure and Dynamics*, **30**, pp. 1–9 (2021).

36. Mehbodniya, A., Webber, J.L., Rani, R., et al. "Energy-aware routing protocol with fuzzy logic in industrial internet of things with blockchain technology", *Wireless Communications and Mobile Computing*, **2022**, 7665931 (2022).

37. Ramalingam, P., Mehbodniya, A., Webber, J.L., et al. "Telemetry data compression algorithm using balanced recurrent neural network and deep learning", *Computational Intelligence and Neuroscience*, **2022**, 4886586 (2022).

38. Webber, J., Mehbodniya, A., Teng, R., et al. "Finger-gesture recognition for visible light communication systems using machine learning", *Applied Sciences*, **11**(24), 11582 (2021).

39. Roozitalab, A. "Investigating the relationship between managers' leadership styles (based on Likert theory) and employees' job satisfaction in jumbo Chain Stores Branches in the Tehran city", *EFFLATOUNIA-Multidisciplinary Journal*, **5**(2), pp. 3271–3280 (2021).

40. Taghibeikzadehbadr, P., Shabkhiz, F., and Shahrbanian, S. "Expression of PGC-1 alpha isoforms in response to eccentric and concentric resistance training in healthy subjects", *Journal of Sport Biosciences*, **11**(4), pp. 447–462 (2020).

41. Sabouri, M., Kordi, M., Shabkhiz, F., et al. "Moderate treadmill exercise improves spatial learning and memory deficits possibly via changing PDE-5, IL-1 β and pCREB expression", *Experimental Gerontology*, **139**, 111056 (2020).

42. Molaei, S., Ghorbani, N., Dashtiahangar, F., et al. "FDCNet: Presentation of the fuzzy CNN and fractal feature extraction for detection and classification of tumors", *Computational Intelligence and Neuroscience*, **2022**, 7543429 (2022).

43. Roozitalab, A. and Majidi, M. "Factors affecting on improvement employee empowerment: Case study: Saipa corporation", *International Review*, **1-2**, pp. 9–17 (2017).

44. Esmaeilion, F., Ahmadi, A., and Dashti, R. "Exergy-economic-environment optimization of the waste-to-energy power plant using multi-objective particle-swarm optimization (MOPSO)", *Scientia Iranica*, **28**(5), pp. 2733–2750 (2021).

45. Coskun, A., Bolatturk, A., and Kanoglu, M. "Thermodynamic and economic analysis and optimization of power cycles for a medium temperature geothermal resource", *Energy Conversion and Management*, **78**, pp. 39–49 (2014).

Biographies

Farshid Mehran received his BSc in Mechanical Engineering and has worked in different areas including fluid mechanics and thermodynamics in Department of Mechanical Engineering, Islamic Azad university, Jolfa International branch, Jolfa, Iran. He completed his MSc in Mechanical Engineering from Islamic Azad University. His research interests are non-Newton fluids, micro-fluids, and computational fluid dynamics.

Yasman Parvizifard received her MSc in Mechanical Engineering from University College of Nabi Akram,

Tabriz, Iran. Her research interests are fluid mechanics, computational fluid dynamics, and nano-fluids. Now, she is working as a researcher in the field of fluid mechanics and computational fluid mechanics.

Farhad Hassanzadeh is an MSc graduate in Mechanical Engineering from Islamic Azad University. He is a researcher in the Engine and Thermal Systems at the Department of Mechanical Engineering. His current research interests are the computational fluid dynamics, fluid flow, and heat transfer.

Nikolay Kuznetsov is a Doctor of Economics, Director of the Center for Strategic Forecasting and Planning of the Financial University under the Government of the Russian Federation. He defended his doctoral thesis in 2016 and has taught finance theory, financial analysis, and financial modeling. His main research interests include financial management, strategic management, financial analytics, modeling, and forecasting.